Available online at www.sciencedirect.com
ScienceDirect
Computers and Mathematics with Applications 55 (2008) 1706–1719
An International Journal
computers & mathematics
with applications
www.elsevier.com/locate/camwa

Triangular subpatches of rectangular Bézier surfaces

Dieter Lasser

Computer Graphics & CAGD, Drosselweg 7, 64409 Messel, Germany

Received 7 August 2006; received in revised form 7 April 2007; accepted 10 April 2007

Abstract

A formula is presented for describing triangular subpatches of rectangular Bézier surfaces. Calculations using it are numerically stable, since they are based on de Casteljau recursions and convex combinations of combinatorial constants. Several examples of quadratic, cubic and quartic subpatches are given, and the bi- and the quadripartition of a rectangular Bézier surface are discussed.

Keywords: Bézier surfaces; Subpatches; Surfaces on surfaces; Composition; Conversion; Corner cutting; Bipartitioning; Quadripartitioning

1. Introduction

Surfaces on surfaces can be looked at as subpatches of surfaces with boundary curves that are (in general) not isoparametric. These subpatches might be created through typical surface interrogation techniques such as intersecting, blending or trimming. It is advantageous to be able to define these patches exactly using common Bézier methods, instead of employing numerical approximations. Surface composition applied in this paper offers one suitable solution. Further applications of methods and results presented are free form deformation, [1, Chap. 11.5] and product labeling (i.e. attaching a label to an article). Labeling might involve *arbitrary shaped* subsegments of a surface which ought to be described by triangle and/or tensor product Bézier (briefly TB and TPB) representations. Multi-patch surfaces, [1, Chap. 7.5, 7.6], provide further usage, since, subdivision, reparametrization and continuity constructions are possible applications of composition. Therefore, problems such as the N-sided hole (e.g. the suitcase corner), [1, p. 314, 331, 354], the N-sided vertex, [1, p. 330, 356], or the T-node surface configuration, [1, p. 353], could be addressed. Finally, because of the variety of modelling systems in operation, some of which are using rectangular while others are using tringular schemes, the need for a stable, reliable method for conversion from three-sided to four-sided surface types (and conversely) defines one more very important application of formulas presented within this manuscript.

Rectangular and triangular Bézier surfaces are among the most commonly used surfaces in CAGD. Thus, there are four potential combinations of forms to define surfaces on surfaces: two cases of combining equal shapes and two of combining diverse shapes. Publications on TB representations, which are very well understood, date back to the years 1983 and 1984 [2–4]. Ideas and concepts have been reformulated and worked on later using blossoming and functional composition principles, [5–8]. TPB representations are the subject of [9]. Combinations of diverse shapes

E-mail address: lasser@t-online.de.

0898-1221/$ - see front matter
doi:10.1016/j.camwa.2007.04.049

are trickier. Brueckner, [10], converts a TB surface to a trimmed TPB surface, Waggenspack and Anderson, [11], exactly transform a monomial to a TB representation, and Jie, [12], extends the equations to rationals. The explicit formula of Goldman and Filip, [13], converts a TPB surface of degree (m, n) into two TB surfaces of degree $m + n$. Lino and Wilde [14], decompose a TB surface into three rational TPB surfaces. Hu, [15], represents a TB surface as a degenerated TPB surface using corner cutting methods and addresses in 1996, [16], the suitcase corner problem by applying a bilinear reparametrization. Feng and Peng, [17], present algorithms for the composition of TPB and TB surfaces through linear barycentric (resp. bilinear) reparametrization. Lasser, in 2002 [18], provides formulas and a geometric algorithm for the conversion of rectangular subpatches of TB surfaces into TPB representation.

In this paper, we discuss triangular shaped Bézier surfaces defined in the domain of rectangular Bézier surfaces. TPB as well as TB surfaces can be of arbitrary polynomial degree, generalizing [13] and [17] which both deal with linear barycentric representations only. Section 2 introduces the notation used throughout this paper by reviewing definitions of TB and TPB representations. Section 3 presents an explicit Bézier representation of triangular subpatches of rectangular Bézier surfaces and sketches a de Casteljau-like algorithm. Section 4 discusses examples such as quadratic, cubic, and quartic triangular subpatches as well as the special problems of bipartitioning and quadripartitioning of TPB surfaces.

2. Bézier representations

A triangle Bézier surface $\mathbf{T}(u, v, w)$ – briefly TB surface – of degree N in (u, v, w) is defined by

$$\mathbf{T}(u, v, w) = \sum_{|\mathbf{I}|=N} \mathbf{T}_{I,J,K} B^N_{I,J,K}(u, v, w) \tag{1}$$

with Bézier points $\mathbf{T}_{I,J,K} \in \mathbb{R}^2$ and with (generalized) Bernstein polynomials

$$B^N_{I,J,K}(u, v, w) = \binom{N}{\mathbf{I}} u^I v^J w^K, \quad \text{where } \binom{N}{\mathbf{I}} = \frac{N!}{I!J!K!}, \tag{2}$$

of degree N in barycentric coordinates $\mathbf{u} = (u, v, w)$ which satisfy $|\mathbf{u}| = u+v+w = 1$ and $0 \le u, v, w \le 1$ associated with a base triangle $\triangle(\mathbf{U}, \mathbf{V}, \mathbf{W})$ of $\mathbf{u}$-parameter space. $\sum_{|\mathbf{I}|=N}$ denotes summation over all triples $\mathbf{I} = (I, J, K)$ which satisfy $|\mathbf{I}| = I + J + K = N$ and $0 \le I, J, K \le N$.

A rectangular Bézier surface $\mathbf{R}(\mu, \nu)$ also called a tensor product Bézier surface – briefly TPB surface – of degree (l, m) in (μ, ν) is defined by

$$\mathbf{R}(\mu, \nu) = \sum_{i=0}^{l} \sum_{j=0}^{m} \mathbf{R}_{i,j} B^l_i(\mu) B^m_j(\nu) \tag{3}$$

with Bézier points $\mathbf{R}_{i,j} \in \mathbb{R}^3$ and with (ordinary) Bernstein polynomials

$$B^l_i(\mu) = \binom{l}{i} \mu^i (1 - \mu)^{l-i} \tag{4}$$

of degree l in μ and $B^m_j(\nu)$ of degree m in ν similarly, $\mu, \nu \in [0, 1]$.

Bézier representations are quite popular because their expansion in terms of Bernstein polynomials yields, first, a numerically very stable behavior of all algorithms and, second, a geometric meaning for the Bézier points. For an extensive coverage of properties of Bernstein polynomials and Bézier representations see e.g. [1,7].

3. Calculation of triangular subpatches

The Bézier representation of triangular subpatches can be derived through the composition of a TB surface $\mathbf{T}(\mathbf{u})$ and a TPB surface $\mathbf{R}(\mu, \nu)$ such that the base triangle of the TB surface is getting mapped into the domain of the TPB surface (Fig. 1). Theorem 1 is fundamental for all applications mentioned above and the ones discussed below if exact and explicit representations are needed.

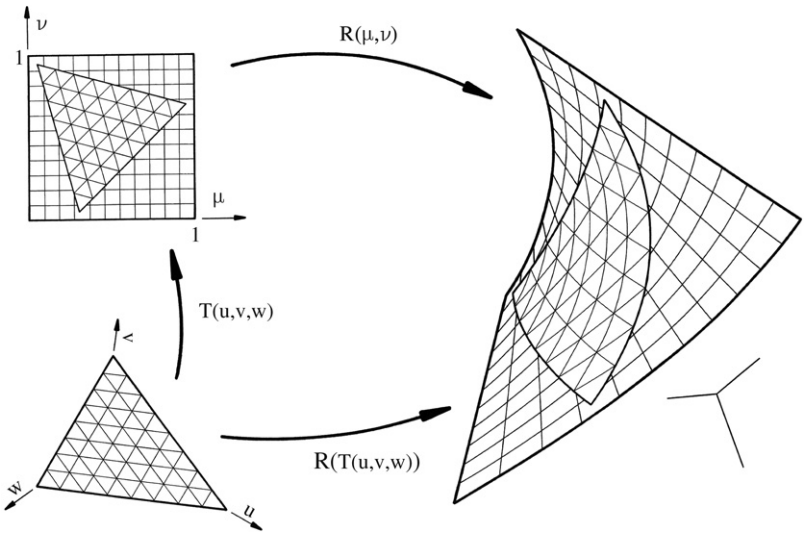

Fig. 1. A triangular on a rectangular Bézier surface using a composition of two mappings.

Theorem 1. *Let* $\mathbf{T}(\mathbf{u}) = (\mu(\mathbf{u}), \nu(\mathbf{u})) : \mathbb{R}^2 \mapsto \mathbb{R}^2$ *be a polynomial TB surface of degree* N *in* $\mathbf{u} = (u, v, w)$, (1), *with Bézier points* $\mathbf{T}_{I,J,K} = (\mu_{I,J,K}, \nu_{I,J,K})$, *and let* $\mathbf{R}(\mu, \nu) = (x(\mu, \nu), y(\mu, \nu), z(\mu, \nu)) : \mathbb{R}^2 \mapsto \mathbb{R}^3$ *be a polynomial TPB surface of degree* (l, m) *in* (μ, ν), (3), *with Bézier points* $\mathbf{R}_{i,j} = (x_{i,j}, y_{i,j}, z_{i,j})$.

The composition $\mathbf{S}(\mathbf{u}) = \mathbf{R}(\mathbf{T}(\mathbf{u})) = \mathbf{R}(\mu(\mathbf{u}), \nu(\mathbf{u}))$ is polynomial and can be represented as a TB surface of degree $N(l + m)$:

$$\mathbf{S}(\mathbf{u}) = \sum_{|\mathbf{I}|=N(l+m)} \mathbf{S}_{\mathbf{I}} B_{\mathbf{I}}^{N(l+m)}(\mathbf{u}) \tag{5}$$

with Bézier points

$$\mathbf{S}_{\mathbf{I}} = \sum_{\mathbf{I}^\mu+\mathbf{I}^\nu=\mathbf{I}} C_{|\mathbf{I}|}^{l+m}(N, \mathbf{I}) \mathbf{R}_{0,0}^{l,m}(\mu_{\mathbf{I}^\mu}^l, \nu_{\mathbf{I}^\nu}^m) \tag{6}$$

and constants

$$C_{|\mathbf{I}|}^{l+m}(N, \mathbf{I}) = \frac{\prod_{Q^\mu=1}^{l} \binom{N}{\mathbf{I}_{Q^\mu}^\mu} \prod_{Q^\nu=1}^{m} \binom{N}{\mathbf{I}_{Q^\nu}^\nu}}{\binom{N(l+m)}{\mathbf{I}}}, \tag{7}$$

$\sum_{|\mathbf{I}|=N(l+m)}$ has the meaning of summation over all index tuples $\mathbf{I} = \mathbf{I}^\mu + \mathbf{I}^\nu$, where $\mathbf{I}^\mu = \mathbf{I}_1^\mu + \cdots + \mathbf{I}_l^\mu$, $\mathbf{I}_{Q^\mu}^\mu = (I_{Q^\mu}^\mu, J_{Q^\mu}^\mu, K_{Q^\mu}^\mu)$ with $|\mathbf{I}_{Q^\mu}^\mu| = I_{Q^\mu}^\mu + J_{Q^\mu}^\mu + K_{Q^\mu}^\mu = N$ and $I_{Q^\mu}^\mu, J_{Q^\mu}^\mu, K_{Q^\mu}^\mu \in \{0, 1, \ldots, N\}$, $\mathbf{I}^\nu$ analogously, and $|\mathbf{I}| = |\mathbf{I}^\mu| + |\mathbf{I}^\nu| = Nl + Nm = N(l + m)$.

Remark 1. Construction points $\mathbf{R}_{0,0}^{l,m}(\mu_{\mathbf{I}^\mu}^l, \nu_{\mathbf{I}^\nu}^m)$ arise in the calculation of the polar form (also known as the blossom) of $\mathbf{R}(\mu, \nu)$. They can be found recursively using the de Casteljau algorithm, for example, in the μ-direction we compute

$$\mathbf{R}_{i,j}^{\alpha,\beta}(\mu_{\mathbf{I}^\mu}^\alpha, \nu_{\mathbf{I}^\nu}^\beta) = (1 - \mu_{\mathbf{I}_\alpha^\mu}) \mathbf{R}_{i,j}^{\alpha-1,\beta}(\mu_{\mathbf{I}^\mu}^{\alpha-1}, \nu_{\mathbf{I}^\nu}^\beta) + \mu_{\mathbf{I}_\alpha^\mu} \mathbf{R}_{i+1,j}^{\alpha-1,\beta}(\mu_{\mathbf{I}^\mu}^{\alpha-1}, \nu_{\mathbf{I}^\nu}^\beta) \tag{8}$$

with a similar recursion in the ν-direction, and the initialization $\mathbf{R}_{i,j}^{0,0} = \mathbf{R}_{i,j}$ where $\mathbf{I}^\mu$ symbolizes indices $\mathbf{I}_1^\mu, \ldots, \mathbf{I}_\alpha^\mu$, on the left side, while on the right side, $\mathbf{I}^\mu$ symbolizes indices $\mathbf{I}_1^\mu, \ldots, \mathbf{I}_{\alpha-1}^\mu$. $\mathbf{I}^\nu$ symbolizes indices $\mathbf{I}_1^\nu, \ldots, \mathbf{I}_\beta^\nu$ on both

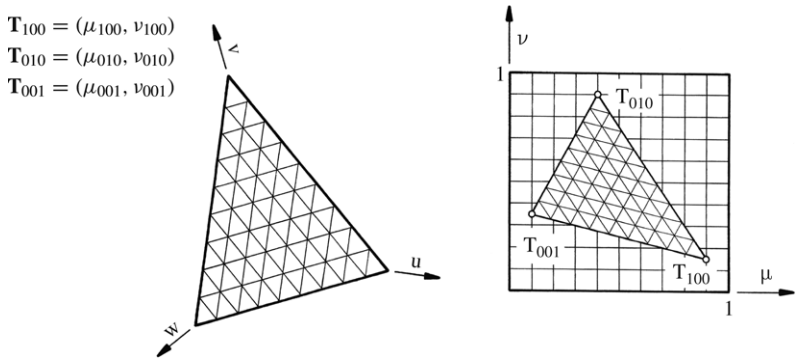

Fig. 2. Linearly parametrized triangular subdomain of the μ–ν-domain of a TPB surface.

sides of the recursion equation. Therefore, the calculation of $\mathbf{R}_{i,j}^{\alpha,\beta}(\mu_{\mathbf{I}^\mu}^{\alpha}, \nu_{\mathbf{I}^\nu}^{\beta})$ implies α de Casteljau constructions for parameter values $\mu_{\mathbf{I}_1^\mu}, \mu_{\mathbf{I}_2^\mu}, \ldots, \mu_{\mathbf{I}_\alpha^\mu}$ and β de Casteljau constructions for parameter values $\nu_{\mathbf{I}_1^\nu}, \nu_{\mathbf{I}_2^\nu}, \ldots, \nu_{\mathbf{I}_\beta^\nu}$. Note, the blossom of $\mathbf{R}(\mu, \nu)$ is symmetric w.r.t. the argument.

The proof of Theorem 1 is basically like the one given in detail in [18].

4. Quadratic, cubic and quartic subpatches

While Theorem 1 in its generality handles arbitrary polynomial degrees and therefore addresses all applications mentioned in the Introduction, in some special cases the computational costs reduce drastically and the equations simplify a lot; eventually even explicit formulas for control points can be derived. This is especially true for the case $N = 1$ which describes a surface subpatch corresponding to a linearly parametrized triangular subdomain of the domain of the TPB surface (Fig. 2).

4.1. Quadratic triangular subpatches

Quadratic triangular subpatches can be found in general only on bilinear TPB surfaces, i.e. $l = m = 1$, if $N = 1$. Bilinear TPB surfaces define rectangular surfaces which linearly interpolate the boundary of a quadrilateral in space. They describe segments of hyperbolic paraboloidal surfaces (also known as hypar surfaces).

For $l = m = 1$ and $N = 1$ we have $\mathbf{I}^\mu = \mathbf{I}_1^\mu = (I_1^\mu, J_1^\mu, K_1^\mu)$ with $|\mathbf{I}_1^\mu| = I_1^\mu + J_1^\mu + K_1^\mu = 1$ and $I_1^\mu, J_1^\mu, K_1^\mu \in \{0, 1\}$, i.e. there are just three different index triples $\mathbf{I}_1^\mu$: (1, 0, 0), (0, 1, 0) and (0, 0, 1), and similarly for $\mathbf{I}^\nu$, and therefore (7) reduces to

$$C_{|\mathbf{I}|}^2(1, \mathbf{I}) = \frac{\binom{1}{\mathbf{I}_1^\mu}\binom{1}{\mathbf{I}_1^\nu}}{\binom{2}{\mathbf{I}}} = \frac{1}{\binom{2}{\mathbf{I}}},$$

with $\mathbf{I} = \mathbf{I}^\mu + \mathbf{I}^\nu = \mathbf{I}_1^\mu + \mathbf{I}_1^\nu$, $|\mathbf{I}| = 2$, and Eqs. (5) and (6) of Theorem 1 simplify to

$$\mathbf{S}(\mathbf{u}) = \sum_{|\mathbf{I}|=2} \mathbf{S}_\mathbf{I} B_\mathbf{I}^2(\mathbf{u}) \tag{9}$$

and

$$\mathbf{S}_\mathbf{I} = \frac{1}{\binom{2}{\mathbf{I}}} \sum_{\mathbf{I}^\mu + \mathbf{I}^\nu = \mathbf{I}} \mathbf{R}_{00}^{11}(\mu_{\mathbf{I}_1^\mu}, \nu_{\mathbf{I}_1^\nu}). \tag{10}$$

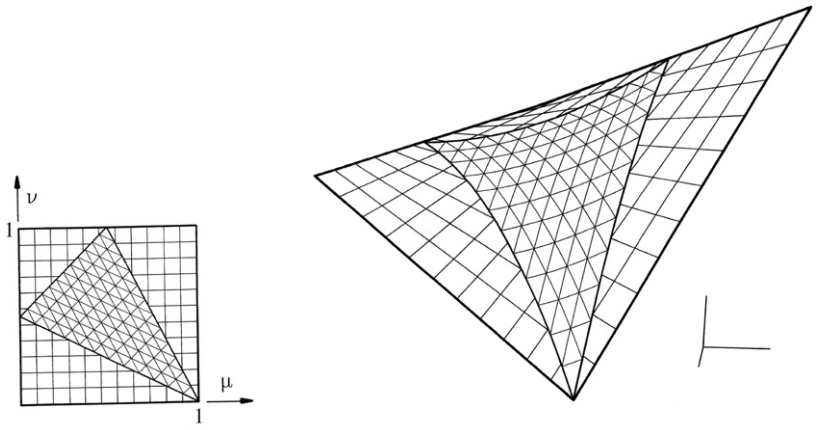

Fig. 3. A quadratic triangular subpatch of a hyperbolic paraboloidal TPB surface.

In detail, Eq. (10) gives the Bézier points of a quadratic TB subpatch of a bilinear TPB surface (Fig. 3)

$$\begin{aligned}
\mathbf{S}_{200} &= \mathbf{R}_{00}^{11}(\mu_{100}, \nu_{100}),\\
\mathbf{S}_{020} &= \mathbf{R}_{00}^{11}(\mu_{010}, \nu_{010}),\\
\mathbf{S}_{002} &= \mathbf{R}_{00}^{11}(\mu_{001}, \nu_{001}),\\
\mathbf{S}_{110} &= \frac{1}{2}\left[\mathbf{R}_{00}^{11}(\mu_{100}, \nu_{010}) + \mathbf{R}_{00}^{11}(\mu_{010}, \nu_{100})\right],\\
\mathbf{S}_{101} &= \frac{1}{2}\left[\mathbf{R}_{00}^{11}(\mu_{100}, \nu_{001}) + \mathbf{R}_{00}^{11}(\mu_{001}, \nu_{100})\right],\\
\mathbf{S}_{011} &= \frac{1}{2}\left[\mathbf{R}_{00}^{11}(\mu_{010}, \nu_{001}) + \mathbf{R}_{00}^{11}(\mu_{001}, \nu_{010})\right].
\end{aligned} \tag{11}$$

4.2. Cubic triangular subpatches

Cubic triangular subpatches can be found in general only on TPB surfaces which are linear in one and quadratic in the other parameter direction, describing segments of parabolic cylinders, if $N = 1$. W.l.o.g. we set $l = 1$, $m = 2$, yielding

$$C^3_{|\mathbf{I}|}(1, \mathbf{I}) = \frac{\binom{1}{\mathbf{I}_1^\mu}\binom{1}{\mathbf{I}_1^\nu}\binom{1}{\mathbf{I}_2^\nu}}{\binom{3}{\mathbf{I}}} = \frac{1}{\binom{3}{\mathbf{I}}},$$

and Eqs. (5) and (6) simplify to

$$\mathbf{S}(\mathbf{u}) = \sum_{|\mathbf{I}|=3} \mathbf{S}_\mathbf{I} B^3_\mathbf{I}(\mathbf{u}) \tag{12}$$

with

$$\mathbf{S}_\mathbf{I} = \frac{1}{\binom{3}{\mathbf{I}}} \sum_{\mathbf{I}^\mu + \mathbf{I}^\nu = \mathbf{I}} \mathbf{R}_{00}^{12}(\mu_{\mathbf{I}_1^\mu}, \nu_{\mathbf{I}_1^\nu}, \nu_{\mathbf{I}_2^\nu}). \tag{13}$$

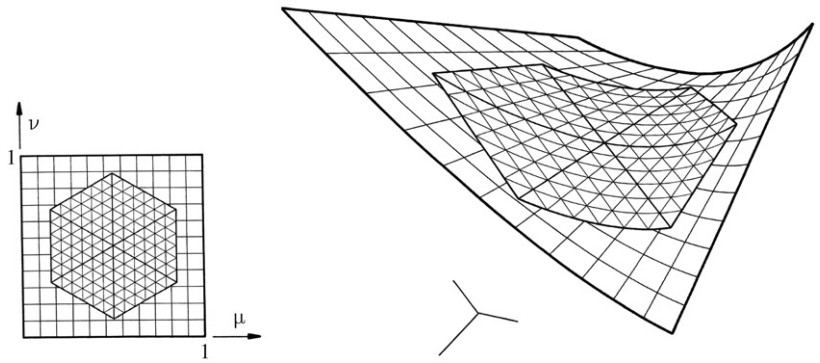

Fig. 4. Six cubic triangular subpatches of a TPB surface forming a hexagon.

Thus, the Bézier points $\mathbf{S_I}$ of the cubic TB subpatch are (Fig. 4 shows an application)

$$\begin{aligned}
\mathbf{S}_{300} &= \mathbf{R}^{12}_{00}(\mu_{100}, \nu_{100}, \nu_{100}),\\
\mathbf{S}_{030} &= \mathbf{R}^{12}_{00}(\mu_{010}, \nu_{010}, \nu_{010}),\\
\mathbf{S}_{003} &= \mathbf{R}^{12}_{00}(\mu_{001}, \nu_{001}, \nu_{001}),\\
\mathbf{S}_{210} &= \frac{1}{3}\left[\mathbf{R}^{12}_{00}(\mu_{010}, \nu_{100}, \nu_{100}) + 2\mathbf{R}^{12}_{00}(\mu_{100}, \nu_{100}, \nu_{010})\right],\\
\mathbf{S}_{201} &= \frac{1}{3}\left[\mathbf{R}^{12}_{00}(\mu_{001}, \nu_{100}, \nu_{100}) + 2\mathbf{R}^{12}_{00}(\mu_{100}, \nu_{100}, \nu_{001})\right],\\
\mathbf{S}_{120} &= \frac{1}{3}\left[\mathbf{R}^{12}_{00}(\mu_{100}, \nu_{010}, \nu_{010}) + 2\mathbf{R}^{12}_{00}(\mu_{010}, \nu_{100}, \nu_{010})\right],\\
\mathbf{S}_{102} &= \frac{1}{3}\left[\mathbf{R}^{12}_{00}(\mu_{100}, \nu_{001}, \nu_{001}) + 2\mathbf{R}^{12}_{00}(\mu_{001}, \nu_{100}, \nu_{001})\right],\\
\mathbf{S}_{021} &= \frac{1}{3}\left[\mathbf{R}^{12}_{00}(\mu_{001}, \nu_{010}, \nu_{010}) + 2\mathbf{R}^{12}_{00}(\mu_{010}, \nu_{010}, \nu_{001})\right],\\
\mathbf{S}_{012} &= \frac{1}{3}\left[\mathbf{R}^{12}_{00}(\mu_{010}, \nu_{001}, \nu_{001}) + 2\mathbf{R}^{12}_{00}(\mu_{001}, \nu_{010}, \nu_{001})\right],\\
\mathbf{S}_{111} &= \frac{1}{3}\left[\mathbf{R}^{12}_{00}(\mu_{100}, \nu_{010}, \nu_{001}) + \mathbf{R}^{12}_{00}(\mu_{010}, \nu_{100}, \nu_{001}) + \mathbf{R}^{12}_{00}(\mu_{001}, \nu_{100}, \nu_{010})\right].
\end{aligned} \tag{14}$$

4.3. Quartic triangular subpatches

There are three ways to form quartic triangular subpatches of TPB surfaces: First, if $N = 1$, describing subsegments of elliptic paraboloids, i.e. as subsegments of biquadratic TPB surfaces (Section 4.3.1); second, if $N = 1$, describing subsegments of cubic cylinders, i.e. as subsegments of TPB surfaces which are linear in one and cubic in the other parameter direction (Section 4.3.2); and third, if $N = 2$, describing subsegments of hyperbolic paraboloids (hypar surface, also called saddle surface), i.e. as subsegments of bilinear TPB surfaces (Section 4.3.3).

4.3.1. Quartic triangular subpatches of biquadratic TPB surfaces

For $l = m = 2$ and $N = 1$ combinatorial constants $C^{l+m}_{|\mathbf{I}|}(N, \mathbf{I})$ simplify, similarly to Sections 4.1 and 4.2, and Bézier points $\mathbf{S_I}$, (6),

$$\mathbf{S_I} = \frac{1}{\binom{4}{\mathbf{I}}} \sum_{\mathbf{I}^\mu + \mathbf{I}^\nu = \mathbf{I}} \mathbf{R}^{22}_{00}(\mu_{\mathbf{I}^\mu_1}, \mu_{\mathbf{I}^\mu_2}, \nu_{\mathbf{I}^\nu_1}, \nu_{\mathbf{I}^\nu_2}). \tag{15}$$

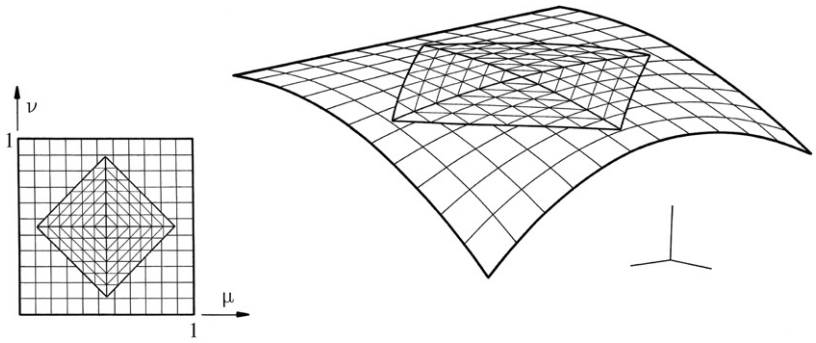

Fig. 5. Four quartic triangular subpatches of a biquadratic TPB surface forming a diamond-shaped subsegment.

of the quartic TB subpatch are calculated by (Fig. 5 shows an application)

$$
\begin{aligned}
\mathbf{S}_{400} &= \mathbf{R}^{22}_{00}(\mu_{100},\mu_{100},\nu_{100},\nu_{100}),\\
\mathbf{S}_{040} &= \mathbf{R}^{22}_{00}(\mu_{010},\mu_{010},\nu_{010},\nu_{010}),\\
\mathbf{S}_{004} &= \mathbf{R}^{22}_{00}(\mu_{001},\mu_{001},\nu_{001},\nu_{001}),\\
\mathbf{S}_{310} &= \frac{1}{2}\left[\mathbf{R}^{22}_{00}(\mu_{100},\mu_{100},\nu_{100},\nu_{010})+\mathbf{R}^{22}_{00}(\mu_{100},\mu_{010},\nu_{100},\nu_{100})\right],\\
\mathbf{S}_{301} &= \frac{1}{2}\left[\mathbf{R}^{22}_{00}(\mu_{100},\mu_{100},\nu_{100},\nu_{001})+\mathbf{R}^{22}_{00}(\mu_{100},\mu_{001},\nu_{100},\nu_{100})\right],\\
\mathbf{S}_{130} &= \frac{1}{2}\left[\mathbf{R}^{22}_{00}(\mu_{100},\mu_{010},\nu_{010},\nu_{010})+\mathbf{R}^{22}_{00}(\mu_{010},\mu_{010},\nu_{100},\nu_{010})\right],\\
\mathbf{S}_{103} &= \frac{1}{2}\left[\mathbf{R}^{22}_{00}(\mu_{100},\mu_{001},\nu_{001},\nu_{001})+\mathbf{R}^{22}_{00}(\mu_{001},\mu_{001},\nu_{100},\nu_{001})\right],\\
\mathbf{S}_{031} &= \frac{1}{2}\left[\mathbf{R}^{22}_{00}(\mu_{010},\mu_{010},\nu_{010},\nu_{001})+\mathbf{R}^{22}_{00}(\mu_{010},\mu_{001},\nu_{010},\nu_{010})\right],\\
\mathbf{S}_{013} &= \frac{1}{2}\left[\mathbf{R}^{22}_{00}(\mu_{010},\mu_{001},\nu_{001},\nu_{001})+\mathbf{R}^{22}_{00}(\mu_{001},\mu_{001},\nu_{010},\nu_{001})\right],\\
\mathbf{S}_{220} &= \frac{1}{6}\left[\mathbf{R}^{22}_{00}(\mu_{100},\mu_{100},\nu_{010},\nu_{010})+4\mathbf{R}^{22}_{00}(\mu_{100},\mu_{010},\nu_{100},\nu_{010})+\mathbf{R}^{22}_{00}(\mu_{010},\mu_{010},\nu_{100},\nu_{100})\right],\\
\mathbf{S}_{202} &= \frac{1}{6}\left[\mathbf{R}^{22}_{00}(\mu_{100},\mu_{100},\nu_{001},\nu_{001})+4\mathbf{R}^{22}_{00}(\mu_{100},\mu_{001},\nu_{100},\nu_{001})+\mathbf{R}^{22}_{00}(\mu_{001},\mu_{001},\nu_{100},\nu_{100})\right],\\
\mathbf{S}_{022} &= \frac{1}{6}\left[\mathbf{R}^{22}_{00}(\mu_{010},\mu_{010},\nu_{001},\nu_{001})+4\mathbf{R}^{22}_{00}(\mu_{010},\mu_{001},\nu_{010},\nu_{001})+\mathbf{R}^{22}_{00}(\mu_{001},\mu_{001},\nu_{010},\nu_{010})\right],\\
\mathbf{S}_{211} &= \frac{1}{6}\Big[\mathbf{R}^{22}_{00}(\mu_{100},\mu_{100},\nu_{010},\nu_{001})+2\mathbf{R}^{22}_{00}(\mu_{100},\mu_{010},\nu_{100},\nu_{001})\\
&\quad+\mathbf{R}^{22}_{00}(\mu_{010},\mu_{001},\nu_{100},\nu_{100})+2\,\mathbf{R}^{22}_{00}(\mu_{100},\mu_{001},\nu_{100},\nu_{010})\Big],\\
\mathbf{S}_{121} &= \frac{1}{6}\Big[\mathbf{R}^{22}_{00}(\mu_{010},\mu_{010},\nu_{100},\nu_{001})+2\mathbf{R}^{22}_{00}(\mu_{100},\mu_{010},\nu_{010},\nu_{001})\\
&\quad+\mathbf{R}^{22}_{00}(\mu_{100},\mu_{001},\nu_{010},\nu_{010})+2\,\mathbf{R}^{22}_{00}(\mu_{010},\mu_{001},\nu_{100},\nu_{010})\Big],\\
\mathbf{S}_{112} &= \frac{1}{6}\Big[\mathbf{R}^{22}_{00}(\mu_{001},\mu_{001},\nu_{100},\nu_{010})+2\mathbf{R}^{22}_{00}(\mu_{100},\mu_{001},\nu_{010},\nu_{001})\\
&\quad+\mathbf{R}^{22}_{00}(\mu_{100},\mu_{010},\nu_{001},\nu_{001})+2\,\mathbf{R}^{22}_{00}(\mu_{010},\mu_{001},\nu_{100},\nu_{001})\Big].
\end{aligned}
\tag{16}
$$

4.3.2. Quartic triangular subpatches of TPB surfaces of degree (1, 3)

For $l = 1, m = 3$ and $N = 1$ Bézier points $\mathbf{S_I}$, (6),

$$\mathbf{S_I} = \frac{1}{\binom{4}{\mathbf{I}}} \sum_{\mathbf{I}^\mu + \mathbf{I}^\nu = \mathbf{I}} \mathbf{R}^{13}_{00}(\mu_{\mathbf{I}^\mu_1}, \nu_{\mathbf{I}^\nu_1}, \nu_{\mathbf{I}^\nu_2}, \nu_{\mathbf{I}^\nu_3}). \tag{17}$$

of the quartic TB subpatch are calculated by (Fig. 6 shows an example)

$$\begin{aligned}
\mathbf{S}_{400} &= \mathbf{R}^{13}_{00}(\mu_{100}, \nu_{100}, \nu_{100}, \nu_{100}),\\
\mathbf{S}_{040} &= \mathbf{R}^{13}_{00}(\mu_{010}, \nu_{010}, \nu_{010}, \nu_{010}),\\
\mathbf{S}_{004} &= \mathbf{R}^{13}_{00}(\mu_{001}, \nu_{001}, \nu_{001}, \nu_{001}),\\
\mathbf{S}_{310} &= \frac{1}{4}\left[3\mathbf{R}^{13}_{00}(\mu_{100}, \nu_{100}, \nu_{100}, \nu_{010}) + \mathbf{R}^{13}_{00}(\mu_{010}, \nu_{100}, \nu_{100}, \nu_{100})\right],\\
\mathbf{S}_{301} &= \frac{1}{4}\left[3\mathbf{R}^{13}_{00}(\mu_{100}, \nu_{100}, \nu_{100}, \nu_{001}) + \mathbf{R}^{13}_{00}(\mu_{001}, \nu_{100}, \nu_{100}, \nu_{100})\right],\\
\mathbf{S}_{130} &= \frac{1}{4}\left[3\mathbf{R}^{13}_{00}(\mu_{010}, \nu_{100}, \nu_{010}, \nu_{010}) + \mathbf{R}^{13}_{00}(\mu_{100}, \nu_{010}, \nu_{010}, \nu_{010})\right],\\
\mathbf{S}_{103} &= \frac{1}{4}\left[3\mathbf{R}^{13}_{00}(\mu_{001}, \nu_{100}, \nu_{001}, \nu_{001}) + \mathbf{R}^{13}_{00}(\mu_{100}, \nu_{001}, \nu_{001}, \nu_{001})\right],\\
\mathbf{S}_{031} &= \frac{1}{4}\left[3\mathbf{R}^{13}_{00}(\mu_{010}, \nu_{010}, \nu_{010}, \nu_{001}) + \mathbf{R}^{13}_{00}(\mu_{001}, \nu_{010}, \nu_{010}, \nu_{010})\right],\\
\mathbf{S}_{013} &= \frac{1}{4}\left[3\mathbf{R}^{13}_{00}(\mu_{001}, \nu_{010}, \nu_{001}, \nu_{001}) + \mathbf{R}^{13}_{00}(\mu_{010}, \nu_{001}, \nu_{001}, \nu_{001})\right],\\
\mathbf{S}_{220} &= \frac{1}{2}\left[\mathbf{R}^{13}_{00}(\mu_{100}, \nu_{100}, \nu_{010}, \nu_{010}) + \mathbf{R}^{13}_{00}(\mu_{010}, \nu_{100}, \nu_{100}, \nu_{010})\right],\\
\mathbf{S}_{202} &= \frac{1}{2}\left[\mathbf{R}^{13}_{00}(\mu_{100}, \nu_{100}, \nu_{001}, \nu_{001}) + \mathbf{R}^{13}_{00}(\mu_{001}, \nu_{100}, \nu_{100}, \nu_{001})\right],\\
\mathbf{S}_{022} &= \frac{1}{2}\left[\mathbf{R}^{13}_{00}(\mu_{010}, \nu_{010}, \nu_{001}, \nu_{001}) + \mathbf{R}^{13}_{00}(\mu_{001}, \nu_{010}, \nu_{010}, \nu_{001})\right],\\
\mathbf{S}_{211} &= \frac{1}{4}\left[2\mathbf{R}^{13}_{00}(\mu_{100}, \nu_{100}, \nu_{010}, \nu_{001}) + \mathbf{R}^{13}_{00}(\mu_{010}, \nu_{100}, \nu_{100}, \nu_{001}) + \mathbf{R}^{13}_{00}(\mu_{001}, \nu_{100}, \nu_{100}, \nu_{010})\right],\\
\mathbf{S}_{121} &= \frac{1}{4}\left[2\mathbf{R}^{13}_{00}(\mu_{010}, \nu_{100}, \nu_{010}, \nu_{001}) + \mathbf{R}^{13}_{00}(\mu_{100}, \nu_{010}, \nu_{010}, \nu_{001}) + \mathbf{R}^{13}_{00}(\mu_{001}, \nu_{100}, \nu_{010}, \nu_{010})\right],\\
\mathbf{S}_{112} &= \frac{1}{4}\left[2\mathbf{R}^{13}_{00}(\mu_{001}, \nu_{100}, \nu_{010}, \nu_{001}) + \mathbf{R}^{13}_{00}(\mu_{100}, \nu_{010}, \nu_{001}, \nu_{001}) + \mathbf{R}^{13}_{00}(\mu_{010}, \nu_{100}, \nu_{001}, \nu_{001})\right].
\end{aligned} \tag{18}$$

4.3.3. Quartic triangular subpatches of bilinear TPB surfaces

For $l = m = 1$ and $N = 2$, we have $\mathbf{I}^\mu = \mathbf{I}^\mu_1$, $|\mathbf{I}^\mu_1| = I^\mu_1 + J^\mu_1 + K^\mu_1 = 2$ and $I^\mu_1, J^\mu_1, K^\mu_1 \in \{0, 1, 2\}$, and similarly for $\mathbf{I}^\nu$. (7) becomes

$$C^2_{|\mathbf{I}|}(2, \mathbf{I}) = \frac{\binom{2}{\mathbf{I}^\mu_1}\binom{2}{\mathbf{I}^\nu_1}}{\binom{4}{\mathbf{I}}},$$

and Bézier points $\mathbf{S_I}$, (6),

$$\mathbf{S_I} = \sum_{\mathbf{I}^\mu + \mathbf{I}^\nu = \mathbf{I}} \frac{\binom{2}{\mathbf{I}^\mu_1}\binom{2}{\mathbf{I}^\nu_1}}{\binom{4}{\mathbf{I}}} \mathbf{R}^{11}_{00}(\mu_{\mathbf{I}^\mu_1}, \nu_{\mathbf{I}^\mu_1}) \tag{19}$$

of the quartic TB subpatch are calculated by (Fig. 7 illustrates an example)

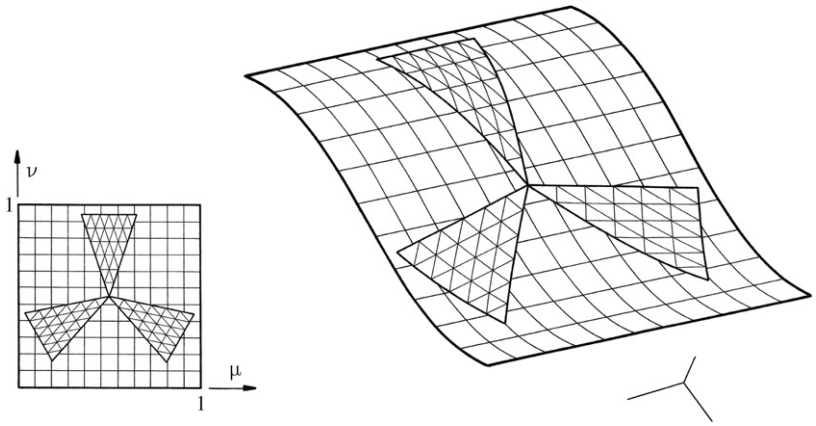

Fig. 6. Three quartic triangular subpatches of a TPB Surface of degree (1, 3).

$$
\begin{aligned}
\mathbf{S}_{400} &= \mathbf{R}_{00}^{11}(\mu_{200}, \nu_{200}),\\
\mathbf{S}_{040} &= \mathbf{R}_{00}^{11}(\mu_{020}, \nu_{020}),\\
\mathbf{S}_{004} &= \mathbf{R}_{00}^{11}(\mu_{002}, \nu_{002}),\\
\mathbf{S}_{310} &= \frac{1}{2}\left[\mathbf{R}_{00}^{11}(\mu_{200}, \nu_{110}) + \mathbf{R}_{00}^{11}(\mu_{110}, \nu_{200})\right],\\
\mathbf{S}_{301} &= \frac{1}{2}\left[\mathbf{R}_{00}^{11}(\mu_{200}, \nu_{101}) + \mathbf{R}_{00}^{11}(\mu_{101}, \nu_{200})\right],\\
\mathbf{S}_{130} &= \frac{1}{2}\left[\mathbf{R}_{00}^{11}(\mu_{020}, \nu_{110}) + \mathbf{R}_{00}^{11}(\mu_{110}, \nu_{020})\right],\\
\mathbf{S}_{103} &= \frac{1}{2}\left[\mathbf{R}_{00}^{11}(\mu_{002}, \nu_{101}) + \mathbf{R}_{00}^{11}(\mu_{101}, \nu_{002})\right],\\
\mathbf{S}_{031} &= \frac{1}{2}\left[\mathbf{R}_{00}^{11}(\mu_{020}, \nu_{011}) + \mathbf{R}_{00}^{11}(\mu_{011}, \nu_{020})\right],\\
\mathbf{S}_{013} &= \frac{1}{2}\left[\mathbf{R}_{00}^{11}(\mu_{002}, \nu_{011}) + \mathbf{R}_{00}^{11}(\mu_{011}, \nu_{002})\right],\\
\mathbf{S}_{220} &= \frac{1}{6}\left[\mathbf{R}_{00}^{11}(\mu_{200}, \nu_{020}) + 4\mathbf{R}_{00}^{11}(\mu_{110}, \nu_{110}) + \mathbf{R}_{00}^{11}(\mu_{020}, \nu_{200})\right],\\
\mathbf{S}_{202} &= \frac{1}{6}\left[\mathbf{R}_{00}^{11}(\mu_{200}, \nu_{002}) + 4\mathbf{R}_{00}^{11}(\mu_{101}, \nu_{101}) + \mathbf{R}_{00}^{11}(\mu_{002}, \nu_{200})\right],\\
\mathbf{S}_{022} &= \frac{1}{6}\left[\mathbf{R}_{00}^{11}(\mu_{020}, \nu_{002}) + 4\mathbf{R}_{00}^{11}(\mu_{011}, \nu_{011}) + \mathbf{R}_{00}^{11}(\mu_{002}, \nu_{020})\right],\\
\mathbf{S}_{211} &= \frac{1}{6}\left[\mathbf{R}_{00}^{11}(\mu_{200}, \nu_{011}) + 2\mathbf{R}_{00}^{11}(\mu_{110}, \nu_{101}) + \mathbf{R}_{00}^{11}(\mu_{011}, \nu_{200}) + 2\mathbf{R}_{00}^{11}(\mu_{101}, \nu_{110})\right],\\
\mathbf{S}_{121} &= \frac{1}{6}\left[\mathbf{R}_{00}^{11}(\mu_{020}, \nu_{101}) + 2\mathbf{R}_{00}^{11}(\mu_{110}, \nu_{011}) + \mathbf{R}_{00}^{11}(\mu_{101}, \nu_{020}) + 2\mathbf{R}_{00}^{11}(\mu_{011}, \nu_{110})\right],\\
\mathbf{S}_{112} &= \frac{1}{6}\left[\mathbf{R}_{00}^{11}(\mu_{002}, \nu_{110}) + 2\mathbf{R}_{00}^{11}(\mu_{101}, \nu_{011}) + \mathbf{R}_{00}^{11}(\mu_{110}, \nu_{002}) + 2\mathbf{R}_{00}^{11}(\mu_{011}, \nu_{101})\right].
\end{aligned}
\tag{20}
$$

4.4. Special problems

The above given formulas of Sections 4.1–4.3 for Bézier points $\mathbf{S_I}$ are programmed and evaluated very easily, though explicit expressions in terms of Bézier points $\mathbf{R}_{i,j}$ are of very high interest as well, because they both reduce computational cost and improve numerical stability. They are provided for the bi- and the quadripartitions of a TPB surface.

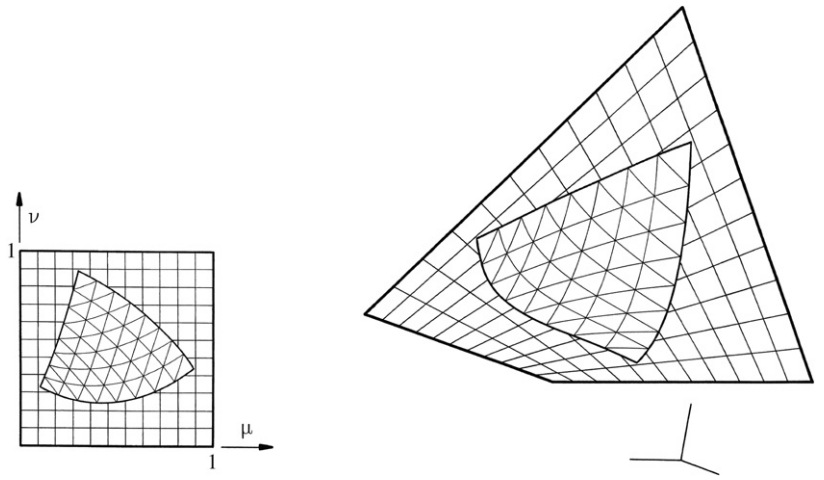

Fig. 7. A quartic triangular subpatch of a hypar surface.

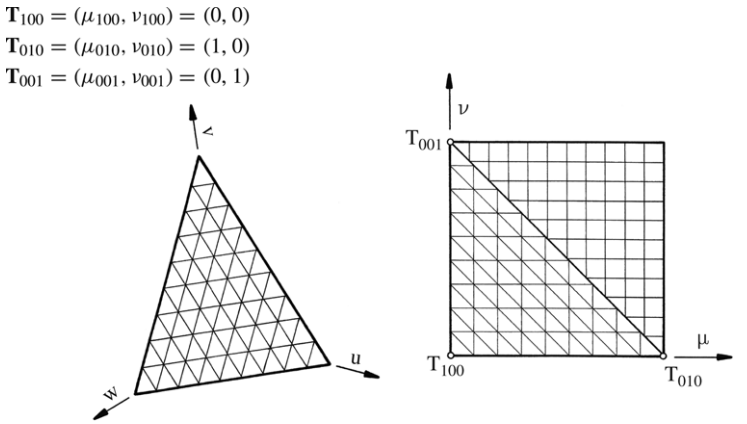

Fig. 8. Domain of $\mathbf{T}(\mathbf{u})$ (left) and half-subpatch $\mathbf{T}(\mathbf{u})$ incl. its defining Bézier points in the μ–ν-domain (right) of a TPB surface.

4.4.1. The bipartition

The bipartition, also known as bisection, divides a TPB surface along one of the diagonals into two triangular segments. To specialize above given equations of Sections 4.1–4.3, we choose control points $\mathbf{T}_{I,J,K}$ according to Fig. 8.

Adapting Eq. (11) of Section 4.1, i.e. situation $l = m = 1$, $N = 1$, to the situation illustrated in Fig. 8, the Bézier points $\mathbf{S_I}$ of the quadratic TB subpatch of the bilinear TPB surface in terms of TPB points $\mathbf{R}_{i,j}$ are

$$\begin{aligned}
\mathbf{S}_{200} &= \mathbf{R}_{00},\\
\mathbf{S}_{020} &= \mathbf{R}_{10},\\
\mathbf{S}_{002} &= \mathbf{R}_{01},\\
\mathbf{S}_{110} &= \frac{1}{2}\left[\mathbf{R}_{00} + \mathbf{R}_{10}\right],\\
\mathbf{S}_{101} &= \frac{1}{2}\left[\mathbf{R}_{01} + \mathbf{R}_{00}\right],\\
\mathbf{S}_{011} &= \frac{1}{2}\left[\mathbf{R}_{11} + \mathbf{R}_{00}\right].
\end{aligned} \tag{21}$$

Similarly, Eq. (14) of Section 4.2, i.e. situation $l = 1$, $m = 2$, $N = 1$, results in the following list of Bézier points $\mathbf{S_I}$ of the cubic TB subpatch of the TPB surface in terms of TPB points $\mathbf{R}_{i,j}$ (Fig. 9).

$$
\begin{aligned}
\mathbf{S}_{300} &= \mathbf{R}_{00},\\
\mathbf{S}_{030} &= \mathbf{R}_{10},\\
\mathbf{S}_{003} &= \mathbf{R}_{02},\\
\mathbf{S}_{210} &= \frac{1}{3}\left[\mathbf{R}_{10} + 2\mathbf{R}_{00}\right],\\
\mathbf{S}_{201} &= \frac{1}{3}\left[\mathbf{R}_{00} + 2\mathbf{R}_{01}\right],\\
\mathbf{S}_{120} &= \frac{1}{3}\left[\mathbf{R}_{00} + 2\mathbf{R}_{10}\right],\\
\mathbf{S}_{102} &= \frac{1}{3}\left[\mathbf{R}_{02} + 2\mathbf{R}_{01}\right],\\
\mathbf{S}_{021} &= \frac{1}{3}\left[\mathbf{R}_{00} + 2\mathbf{R}_{11}\right],\\
\mathbf{S}_{012} &= \frac{1}{3}\left[\mathbf{R}_{12} + 2\mathbf{R}_{01}\right],\\
\mathbf{S}_{111} &= \frac{1}{3}\left[\mathbf{R}_{00} + \mathbf{R}_{01} + \mathbf{R}_{11}\right].
\end{aligned}
\tag{22}
$$

Similarly, in case of the biquadratic TPB surface, Eqs. (15) and (16) of Section 4.3.1, the Bézier points $\mathbf{S_I}$ of the quartic TB subpatch are calculated in terms of Bézier points $\mathbf{R}_{i,j}$ of the TPB surface as follows

$$
\begin{aligned}
\mathbf{S}_{400} &= \mathbf{R}_{00},\\
\mathbf{S}_{040} &= \mathbf{R}_{20},\\
\mathbf{S}_{004} &= \mathbf{R}_{02},\\
\mathbf{S}_{310} &= \frac{1}{2}\left[\mathbf{R}_{00} + \mathbf{R}_{10}\right],\\
\mathbf{S}_{301} &= \frac{1}{2}\left[\mathbf{R}_{01} + \mathbf{R}_{00}\right],\\
\mathbf{S}_{130} &= \frac{1}{2}\left[\mathbf{R}_{10} + \mathbf{R}_{20}\right],\\
\mathbf{S}_{103} &= \frac{1}{2}\left[\mathbf{R}_{02} + \mathbf{R}_{01}\right],\\
\mathbf{S}_{031} &= \frac{1}{2}\left[\mathbf{R}_{21} + \mathbf{R}_{10}\right],\\
\mathbf{S}_{013} &= \frac{1}{2}\left[\mathbf{R}_{12} + \mathbf{R}_{01}\right],\\
\mathbf{S}_{220} &= \frac{1}{6}\left[\mathbf{R}_{00} + 4\mathbf{R}_{10} + \mathbf{R}_{20}\right],\\
\mathbf{S}_{202} &= \frac{1}{6}\left[\mathbf{R}_{02} + 4\mathbf{R}_{01} + \mathbf{R}_{00}\right],\\
\mathbf{S}_{022} &= \frac{1}{6}\left[\mathbf{R}_{22} + 4\mathbf{R}_{11} + \mathbf{R}_{00}\right],\\
\mathbf{S}_{211} &= \frac{1}{6}\left[\mathbf{R}_{01} + 2\mathbf{R}_{11} + \mathbf{R}_{10} + 2\mathbf{R}_{00}\right],\\
\mathbf{S}_{121} &= \frac{1}{6}\left[\mathbf{R}_{21} + 2\mathbf{R}_{11} + \mathbf{R}_{00} + 2\mathbf{R}_{10}\right],\\
\mathbf{S}_{112} &= \frac{1}{6}\left[\mathbf{R}_{00} + 2\mathbf{R}_{01} + \mathbf{R}_{12} + 2\mathbf{R}_{11}\right].
\end{aligned}
\tag{23}
$$

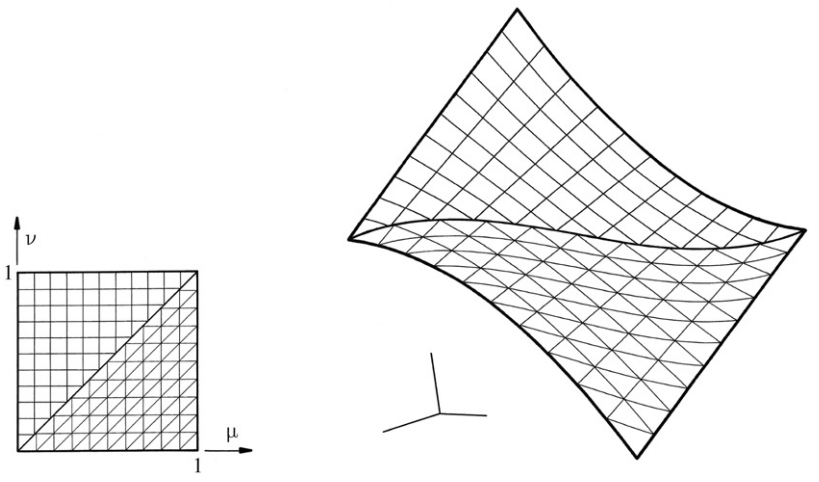

Fig. 9. A triangular cubic subpatch of a TPB surface.

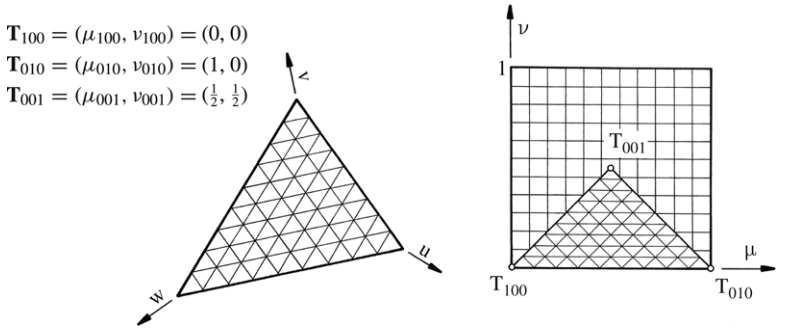

Fig. 10. Domain of $\mathbf{T}(\mathbf{u})$ (left) and quarter-subpatch $\mathbf{T}(\mathbf{u})$, including its defining Bézier points in the μ–ν-domain (right) of a TPB surface.

Rotating the triangular half-subsegment of Fig. 8 (incl. all 3 $\mathbf{T}_{I,J,K}$) around the center point $(\mu, \nu) = (\frac{1}{2}, \frac{1}{2})$ in counterclockwise order provides the Bézier points of the other triangular Bézier subpatches.

4.4.2. The quadripartition

Cutting along both diagonals, the quadripartition divides a TPB surface into four triangular segments. To specialize the above given equations of Sections 4.1–4.3, we choose control points $\mathbf{T}_{I,J,K}$ according to Fig. 10.

TB control points listed in Fig. 10 imply, that Eq. (11) of Section 4.1 specifies such, that the Bézier points $\mathbf{S_I}$ of the quadratic TB subpatch of the bilinear TPB surface are calculated in terms of the TPB points $\mathbf{R}_{i,j}$ as follows (Fig. 11)

$$\begin{aligned}
\mathbf{S}_{200} &= \mathbf{R}_{00},\\
\mathbf{S}_{020} &= \mathbf{R}_{10},\\
\mathbf{S}_{002} &= \frac{1}{4}\left[\mathbf{R}_{00} + \mathbf{R}_{01} + \mathbf{R}_{10} + \mathbf{R}_{11}\right],\\
\mathbf{S}_{110} &= \frac{1}{2}\left[\mathbf{R}_{00} + \mathbf{R}_{10}\right],\\
\mathbf{S}_{101} &= \frac{1}{4}\left[\mathbf{R}_{01} + 2\mathbf{R}_{00} + \mathbf{R}_{10}\right],\\
\mathbf{S}_{011} &= \frac{1}{4}\left[\mathbf{R}_{00} + 2\mathbf{R}_{10} + \mathbf{R}_{11}\right].
\end{aligned} \tag{24}$$

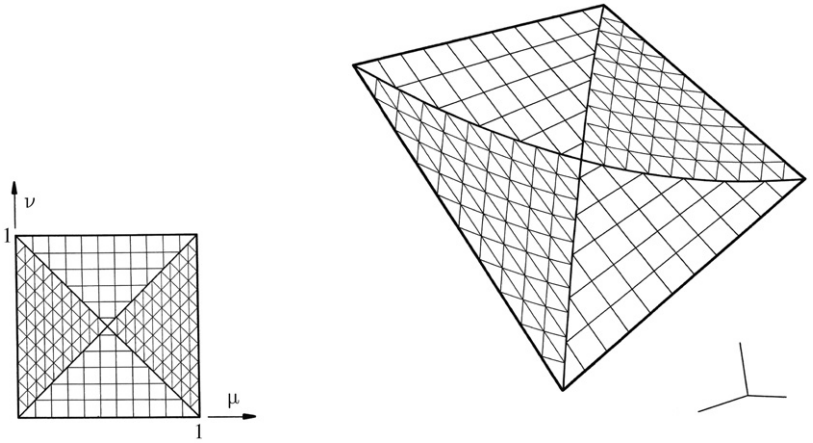

Fig. 11. Two triangular quadratic quarter-subpatches of a bilinear TPB surface.

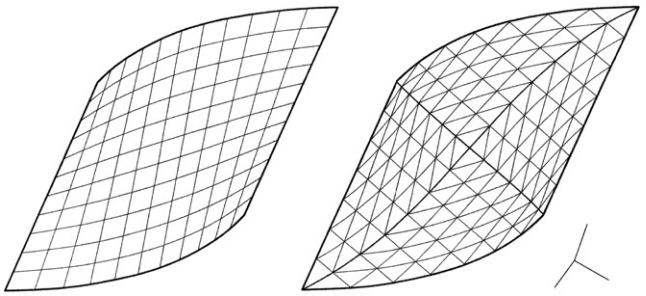

Fig. 12. Four triangular cubic quarter-subpatches (right) of a TPB surface (left).

Similarly, Eq. (14) of Section 4.2 yields the following Bézier points $\mathbf{S_I}$ of the cubic TB subpatch of the TPB surface in terms of TPB points $\mathbf{R}_{i,j}$ (Fig. 12 illustrates a quadripartition)

$$
\begin{aligned}
\mathbf{S}_{300} &= \mathbf{R}_{00},\\
\mathbf{S}_{030} &= \mathbf{R}_{10},\\
\mathbf{S}_{003} &= \frac{1}{8}\left[\mathbf{R}_{00}+\mathbf{R}_{10}+2\mathbf{R}_{01}+2\mathbf{R}_{11}+\mathbf{R}_{02}+\mathbf{R}_{12}\right],\\
\mathbf{S}_{210} &= \frac{1}{3}\left[2\mathbf{R}_{00}+\mathbf{R}_{10}\right],\\
\mathbf{S}_{201} &= \frac{1}{6}\left[2\mathbf{R}_{01}+3\mathbf{R}_{00}+\mathbf{R}_{10}\right],\\
\mathbf{S}_{120} &= \frac{1}{3}\left[2\mathbf{R}_{10}+\mathbf{R}_{00}\right],\\
\mathbf{S}_{102} &= \frac{1}{12}\left[4\mathbf{R}_{01}+2\mathbf{R}_{10}+3\mathbf{R}_{00}+2\mathbf{R}_{11}+\mathbf{R}_{02}\right],\\
\mathbf{S}_{021} &= \frac{1}{6}\left[3\mathbf{R}_{10}+2\mathbf{R}_{11}+\mathbf{R}_{00}\right],\\
\mathbf{S}_{012} &= \frac{1}{12}\left[3\mathbf{R}_{10}+2\mathbf{R}_{00}+4\mathbf{R}_{11}+2\mathbf{R}_{01}+\mathbf{R}_{12}\right],\\
\mathbf{S}_{111} &= \frac{1}{6}\left[2\mathbf{R}_{00}+\mathbf{R}_{01}+2\mathbf{R}_{10}+\mathbf{R}_{11}\right].
\end{aligned}
\tag{25}
$$

Rotating the triangular quarter-subsegment of Fig. 10 (incl. all 3 $\mathbf{T}_{I,J,K}$) around the center point $(\mu, \nu) = (\frac{1}{2}, \frac{1}{2})$ in counterclockwise order provides the Bézier points of the other tringular Bézier subpatches.

Explicit formulas for the control points of the quadripartition for the situation of Section 4.3.1 are available and can be provided upon request.

5. Final remarks

This paper deals with triangular Bézier subpatches of rectangular Bézier surfaces, both of arbitrary polynomial degree. Calculations apply de Casteljau-like recursions forming convex linear combinations of control points. Thus, the numerically stable constructions can also be looked at as a corner cutting algorithm. Some special examples and problems such as quadratic, cubic, and quartic subpatches and the bi- and the quadripartitions are discussed and illustrated, and formulas for Bézier points $\mathbf{S_I}$ of TB surfaces are presented. Quintic triangular subpatches might appear in just two different situations: first, for $l = 1, m = 4$ (or vice versa) and $N = 1$ and, second, for $l = 2, m = 3$ (or vice versa) and $N = 1$. Sixth-degree triangular subpatches show up more often, in five different situations, also including the case of bicubic (i.e. $l = m = 3$) TPB surfaces, [13]. The appearance of seventh-degree subpatches is more restricted again, as is the case for all primes. Calculations and constructions can be carried over easily to multivariate Bézier representations describing volumes and hypersurfaces, (see e.g. [1]), and, using homogeneous coordinates, to rational representations as well.

Acknowledgments

I would like to express my appreciation to the referees for several helpful suggestions to improve the quality and readability of the manuscript.

As highlighted by one of the referees, the bi- and the quadripartition of tensor product surfaces as described above support potential applications in areas such as computer graphics, for illumination models, and multiresolution schemes for instance. This is because current computer graphical cards mostly rely on the triangular structure as the basic primitive.

References

[1] J. Hoschek, D. Lasser, Fundamentals of Computer Aided Geometric Design, AK Peters, Wellesley, 1993.
[2] W. Boehm, G. Farin, Concerning subdivision of Bézier triangles, Computer-Aided Design 15 (5) (1983) 260–261 (Letter to the Editor).
[3] W. Boehm, G. Farin, J. Kahmann, A survey of curve and surface methods in CAGD, Computer Aided Geometric Design 1 (1) (1984) 1–60.
[4] R.N. Goldman, Subdivision algorithms for Bézier triangles, Computer-Aided Design 15 (3) (1983) 159–166.
[5] T.D. DeRose, Composing Bézier simplices, ACM Transactions on Graphics 7 (3) (1988) 198–221.
[6] T.D. DeRose, R.N. Goldman, H. Hagen, S. Mann, Functional composition algorithms via blossoming, ACM Transactions on Graphics 12 (2) (1993) 113–135.
[7] G. Farin, Curves and surfaces for CAGD, in: A Practical Guide, 5th ed., Morgan Kaufmann, 2001.
[8] H.P. Seidel, A general subdivision theorem for Bézier triangles, in: T. Lyche, L.L. Schumaker (Eds.), Mathematical Methods in Computer Aided Geometric Design, Academic Press, San Diego, 1989, pp. 573–581.
[9] D. Lasser, Composition of tensor product Bézier representations, in: G. Farin, H. Hagen, H. Noltemeier (Eds.), Geometric Modelling, in: Computing Supplementum, vol. 8, 1993, pp. 155–172.
[10] I. Brueckner, Construction of Bézier points of quadrilaterals from those of triangles, Computer-Aided Design 12 (1) (1980) 21–24.
[11] W.N. Waggenspack, D.C. Anderson, Converting standard bivariate polynomials to Bernstein form over arbitrary triangular regions, Computer-Aided Design 18 (10) (1986) 529–532.
[12] T. Jie, A geometric condition for smoothness between adjacent rational Bézier surfaces, Computers in Industry 13 (4) (1990) 355–360.
[13] R.N. Goldman, D.J. Filip, Conversion from Bézier rectangles to Bézier triangles, Computer-Aided Design 19 (1) (1987) 25–27.
[14] L. Lino, J. Wilde, Subdivision of triangular Bézier patches into rectangular Bézier patches, Advances in Design Automation 32 (2) (1991) 1–6.
[15] S.M. Hu, Conversion between two classes of Bézier surfaces and geometric continuity jointing, Applied Mathematics: A Journal of Chinese Universities 8 (1993) 290–299.
[16] S.M. Hu, Conversion of a triangular Bézier patch into three rectangular Bézier patches, Computer Aided Geometric Design 13 (3) (1996) 219–226.
[17] J.Q. Feng, Q.S. Peng, Functional compositions via shifting operators for Bézier patches and their applications, Journal of Software 10 (12) (1999) 1316–1321.
[18] D. Lasser, Tensor product Bézier surfaces on triangle Bézier surfaces, Computer Aided Geometric Design 19 (8) (2002) 625–643.